3DinSAR: Object 3D Localization for Indoor RFID Applications

Lanxin Qiu, Zhuangqin Huang
Beijing University of Technology
qiulanxin@emails.bjut.edu.cn
zhuang@bjut.edu.cn

Niklas Wirström
SICS Swedish ICT
niwi@sics.se

Thiemo Voigt
Uppsala University and
SICS Swedish ICT
thiemo@sics.se

***Abstract*—More and more objects can be identified and sensed with RFID tags. Existing schemes for 2D indoor localization have achieved impressing accuracy. In this paper we propose an accurate 3D localization scheme for objects. Our scheme leverages spatial domain phase difference to estimate the height of objects which is inspired by the phase-based Interferometric Synthetic Aperture Radar (InSAR) height determination theory. We further leverage a density-based spatial clustering method to choose the most likely position and show that it improves the accuracy. Our localization method does not need any reference tags. Only one antenna is required to move in a known way in order to construct the synthetic arrays to implement the locating system. We present experimental results from an indoor office environment with EPC C1G2 passive tags and a COTS RFID reader. Our 3D experiments demonstrate a spatial median error of 0.24 m. This novel 3D localization scheme is a simple, yet promising, solution. We believe that it is especially applicable for both portable readers and transport vehicles.**

***Keywords*-UHF RFID; Phase Based; Indoor Localization; 3D; InSAR**

I. Introduction

Many indoor applications require spatial information about objects. Example applications include item finding, object level mapping and large-scale objects managing in warehouses or libraries. However, traditional solutions for location-based services using 802.11, visible light or acoustics [1], [2], [3] usually focus on the users', i.e., persons' positions rather than the position of objects. Also existing indoor mapping machines using optical methods like cameras and infrared, e.g., Free-your Camera [4], Vocel-CRF [5] do not consider objects as an integral part of the environment, but rather view objects as obstacles.

RFID technology enables the identification and location of objects in our daily life by integration of RFID tags. The RF signals that the tags backscatter include a lot of information about the environment of the objects which can be used to derive the objects' spatial information. Towards this end, Malla et al. [6] have provided an approach for 2D object level mapping using RFID, Wang et al.'s RF-Compass [7] robot can recognize and grab objects and Shangguan et al. [8] use the spatial-temporal phase profiling to locate misplaced books in a library and determine the baggage order on the conveyor belt in an airport.

In this paper, we propose a 3D localization scheme, 3DinSAR, for objects that provides spatial information for indoor RFID applications by analyzing the tag backscatter carrier wave's phase characteristics. In order to keep the complexity low and minimize the effort to integrate our solution into existing systems, our approach does not use reference tags or extra reader antennas in the environment. Our 3D localization scheme is implemented using only one movable antenna. It is applicable to both portable readers and transport vehicles.

Our approach leverages the Interference Synthetic Aperture Radar (InSAR) height determination theory. It extends existing 2D hologram localization schemes [9], [10]. Rather than traversing all the spatial pixels which is time consuming and hence not efficient, we extend the naive hologram localization into a 3D scheme by using the spatial domain phase difference which relates to the wave path difference and the tags' height as additional information. We also consider a density-based spatial clustering method to select the most likely position to improve the accuracy.

We implement our system and evaluate it in an office environment at the university using COTS components. Using real hardware we show that our system achieves a localization accuracy with a spatial median error of 0.24 m. Our main contribution is that we are the first to present real-world results for a 3D RFID-based localization system without any reference tags and extra devices.

This paper proceeds as follows. In Section II we discuss related work. We describe the design of our system model and localization scheme in Section III. Section IV then presents real-world experiments in an indoor office environment with EPC C1G2 passive tags and a COTS RFID reader. Finally, Section V concludes the paper.

II. Related Work

This section presents work that is related to ours. We divide it into two parts: Existing 3D localization methods and Synthetic Aperture Radar (SAR)-based methods.

A. 3D Localization

Trilateration based approaches are the most classic solution since the first RFID-based 3D-localization scheme,

978-1-4673-8807-8/16/$31.00 ©2016 IEEE

SpotON [11], was presented. SpotON estimates the target-to-target distance based on signal strength and applies trilateration to give the target position. 3D-BATL [12] requires four readers that are placed on the vertices of a tetrahedron to estimate the distance. It is also based on the analysis of the signal strength which is assumed to be attenuated by the path loss and a logarithmic shadowing effect. Their results are based on simulations. In real-world scenarios, the localization error of these methods may be higher than in simulation.

Maneesilp et al. proposed a fingerprint approximate approach [13]. Their results show a theoretic accuracy as 2.5 cm. However, it is impractical to integrate hundreds of readers both on the ceiling and the floor as reference positions in reality. Thus, BackPos [14] introduces the technique of hyperbolic positioning into RFID localization without the need of reference anchors. BackPos achieves a mean error distance of 40cm with a standard deviation of 20cm in a 2D environment (results from a 3D environment are not presented).

WISP tag is a new technology to combine RFID and sensors together. Zhao and Smith [3] use a custom passive WISP tag with an acoustic tone-detector that receives and times ultrasound signals under the EPC C1G2 standard and an array of ultrasonic beacons. By measuring the ToA of the ultrasound, the passive tag can determine its 3D location. The system provides a precision of 1.5 cm. The RF signal in this work, however, is only used to power the tag and the localization itself is based on ultrasound.

Compared to the above methods, we aim at using as little additional environmental facilities as possible while gaining a high positioning accuracy.

B. Synthetic Aperture Radar

Utilizing synthetic apertures and holographic methods for RFID localization is a promising approach since the resulting resolution (usually around 0.1m [15], [16]) is significantly higher compared to other methods in 2D environments. Using SAR, coherent superposition of phase values measured by one antenna at multiple locations generates the holographic image. Based on this, a spatial probability density function that reveals the actual RFID tag position is computed. We list some related works.

Scherhaufl et al. [9] propose inverse synthetic aperture radar in a MIMO system to increase the accuracy and robustness of 2D localization for passive RFID tags. One reader with 8 transceiver antennas and a mobile tag constitute the MIMO system. The accuracy in terms of root-mean-square deviation is below 10 cm. Tagoram [10] employs differential augmented hologram to track tag tractor in 2D with a median error distance of 1.4 cm for the controllable case and 12 cm in the uncontrollable case. This approach can be extended to the 3D space, but the computations required increase by a factor of thousand and make it hard to implement Tagoram for the 3D case. PinIt [17] creates a SAR through a mobile antenna to extract the multipath profile for each tag. PinIt's intuition is that the tags located in a similar environment have similar multipath profiles [18]. PinIt requires reference tags that are deployed in the environment. PinIt achieves a mean distance error of around 20 cm in a 3D environment.

Our scheme completely liberates 3D object localization from reference tags and extra devices with a high level accuracy. It is based on the previous works of 2D hologram localization scheme. Inspired by the InSAR height determination theory, we apply spatial domain phase difference to estimate the height of tags.

III. Design

In this section we first formulate the problem. Then we describe different existing approaches used to solve different parts of the problem, and finally we describe how we put these parts together to provide the overall solution.

A. Problem Description

We consider the problem of estimating the 3D location of a passive RFID tag with static position, using phase measurements $\Phi = \{\phi_1, \phi_2, ..., \phi_N\}$ measured at known locations $A = \{A_1, A_2, ..., A_N\}$ along a straight line.

Passive RFID systems communicate using a backscatter link. The phase value is a parameter typically reported by COTS readers, and describes the phase offset in the incoming signal. Suppose d is the 3D spatial distance between the reader and the tag. The measured phase offset reported by the reader can then be expressed as:

$$\phi = \left(\frac{4\pi}{\lambda} d + c + c_{MP}\right) \mod 2\pi \tag{1}$$

where λ is the carrier wavelength and c is a phase latency term introduced by the reader's transmitter, the tag's reflection characteristic and the reader's receiver circuits [10]. c is assumed to be unknown because it can be different for each tag/reader pair. c_{MP} is also unknown and represents the multipath influence on phase measurement.

B. Hologram in a 2D scenario

For 2D localization in the plane that intersects the antenna array and the tag location, we can divide the plane into a WxL grid, and denote each point on the grid by $X_{w,l}$, then we can generate a so-called RF holographic image according to the naive hologram method described by Yang et al. [10], as

$$p_{w,l} = |\sum_{n=1}^{N} P(X_{w,l}, A_n, \phi_n)| \tag{2}$$

$$P(X_{w,l}, A_n, \phi_n) = e^{j((\frac{4\pi}{\lambda}|X_{w,l}A_n|)\, mod(2\pi) - \phi_n)} \tag{3}$$

where $e^{j(\phi)}$ indicates a complex exponential signal with unit amplitude. $p_{w,l}$ is the likelihood index which presents

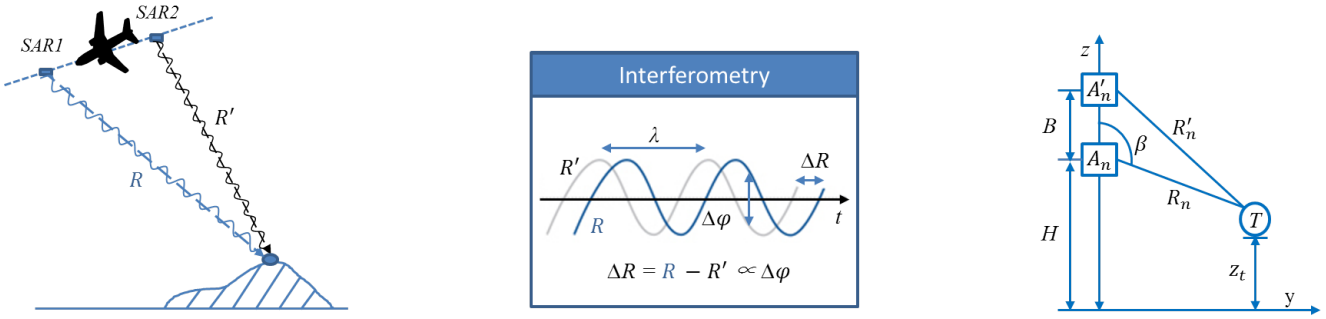

(a) (b) (c)

Figure 1. (a) Height measurement of InSAR. (b) The relationship between transmitter movement and the corresponding shift in signal phase. (c) System structure of 3DinSAR height estimation.

the possibility of grid $X_{w,l}$ is the true tag position. The main concept of the hologram method is that the theoretical phase value should be equal to the measured one for each antenna unit if $X_{w,l}$ is the real location. As a result, by traversing all the $W * L$ pixel in the plane, the point with the maximum $p_{w,l}$ will be selected as the most likely tag position, which means $(x_t, y_t) = (w, l)$. Here, the x-axis is defined to coincide with the antenna array. We also assume that the tag is located in the region for which $y > 0$.

Because the 2D hologram approach gives the location in the plane intersecting the antenna array and the tag's (unknown) location, the 3D interpretation of the solution is a circle around the x-axis at $x = x_t$, with radius equal to l. Hence, we have:

$$l = \sqrt{(y_{A_n} - y_t)^2 + (z_{A_n} - z_t)^2}$$

Here y_{A_n} and z_{A_n} are assumed as the known coordinate value for antenna location A_n when $x_{A_n} = x_t$. The next step is then to find y_t and z_t.

C. InSAR

Interferometric synthetic aperture radar (InSAR) is the measurement of signal phase change between two (or more) SAR images acquired at different positions in order to give the height information of the target point. The distance between the SAR transmitter and target point changes while the signal transmitter moves along a known route. It also leads to a phase value difference which scales up linearly with the distance. Figure 1*(b)* shows the relationship between the transmitter movement and the corresponding shift in signal phase. By detecting the phase difference from the two SAR images, the height information can be inversed according to the geometrical relationship [19]. Inspired by InSAR theory, we consider that the key to find the height information of the target tag for a passive RFID system is by providing an additional phase difference value between two antenna positions with height difference on the fundamental measurements of the 2D hologram.

Now we describe how we find y_t and z_t. Since the tag's x-coordinate x_t can be found through the hologram method described above, we can simplify the 3D problem into 2D as shown in Figure 1*(c)*. The figure shows the plane for which $x = w = x_t$. According to InSAR, we extend our model with an additional phase measurement $\phi_n^{'}$ corresponding to antenna location $A_n^{'}$. $A_n^{'}$ is higher than A_n. A_n is the antenna unit n from the antenna array A, with corresponding measurement ϕ_n. These two antenna units are both with x-coordinates at $x_t = w$.

In the figure, B is the difference along the z-axis between the two antennas, which is called "baseline" in the InSAR theory [19]. H is the z-coordinate of the lower antenna unit, and β is the angle between vector $T - A_n$ and the z-axis. R_n and $R_n^{'}$ are the distances between the antenna units and the tag. As we know, $R_n = l = \sqrt{(y_{A_n} - y_t)^2 + (z_{A_n} - z_t)^2}$ is known from the 2D hologram.

From the figure we see that we can compute the tag's z-coordinate, z_t, as:

$$z_t = H + R_n \cos(\beta) \tag{4}$$

$$\text{where}, \cos(\beta) = \frac{R_n^2 + B^2 - R_n^{'2}}{2R_nB} \tag{5}$$

From InSAR theory we know that:

$$R_n^{'} = R_n + \Delta R \tag{6}$$

$$\Delta R = \frac{\Delta\hat{\phi}}{4\pi}\lambda \tag{7}$$

where $\Delta\hat{\phi}$ is the *real* spatial domain phase difference introduced by the wave path diversity between two transmitters. Then z_t can be described as a function determined and calculated by $z_t = Z(H, B, R_n, \Delta\hat{\phi})$.

However, phase measurements are given as phase difference of the transmitted and received signal modulo 2π. Therefore, here $\Delta\hat{\phi} = \phi_n^{'} - \phi_n + 2k\pi$, where k is an integer related to the antenna and tag positions, and is limited by $|k| \leq \lceil \frac{2B}{\lambda} \rceil$. For each possible k value, when we substitute it into the function of z_t, it will generate a series of possible

tag positions, of which one is the correct position. In fact, each of the possible positions has the same probability and it is impossible to distinguish which one is the correct one.

Although, if we increase our model with a series of additional antenna units at $x = w = x_t$ to create another antenna matrix $A^{'} = \{A_1^{'}, A_2^{'}, ..., A_N^{'}\}$, we can generate candidate points for each combination of A_n and an arbitrary antenna unit from $A^{'}$. In other words, we can obtain several position series with different baselines B. The set of generated points are in general different for the different antenna unit pairs, but have at least one point in common, namely the correct location. We consider to employ the density-based spatial clustering analysis approach to select the target position under one generally true precondition: No matter which the correct k value is, each position series generated by different baselines must have one point corresponding to the real position.

D. Multi-baseline density-based clustering analysis

Density-based spatial clustering of applications with noise (DBSCAN) [20] is a well-known clustering algorithm. The main concept is that given a set of points in space, it groups together points with many nearby neighbors (high-density region) and marks points that lie far away from others as noise (low-density region).

Two important parameters are used to implement this density-based clustering method: the initial scanning radius E and the minimum number of points required to form a dense region $MinPts$. As mentioned above, when the antenna is moved along the z-axis, at $x = w$ to gather another phase measurement collection with different baselines, a set of points P will be generated as described in the previous section. All the point series for different baselines will include the true tag location, or at least close to the practical point with some errors caused by measurement errors. For this reason, the region close to the true location should have the high density. By utilizing DBSCAN, we traverse all the possible points in P, record the number of eligible neighbors and stop when the highest density cluster is found. The other points will be marked as noise. The final tag position can then be computed as the centroid of the highest density cluster.

$$\langle x_t, y_t, z_t \rangle = \frac{\left\langle \sum_i^M x_i, \sum_i^M y_i, \sum_i^M z_i \right\rangle}{M} \tag{8}$$

where M is the number of points in the cluster with highest density.

E. 3D Localization with 3DinSAR

Our complete 3D localization 3DinSAR scheme is depicted in Algorithm 1. It shows that we firstly generate the 2D Naive Hologram. Then based on the result of the 2D holographic image, we apply the InSAR based spatial domain phase difference approach to estimate the possible target positions. At the end, DBSCAN is used to find the highest density region. The final positioning result is given as the centroid of the highest density region. We evaluate the localization accuracy with real world experiments in the next section.

Algorithm 1 3DInSAR Object Localization

Data: Phase measurements from two antenna arrays, and the locations of each antenna unit
Output: Location of the target
Calculate $(x_t, F(y_t, z_t))$ by 2D Naive Hologram with each antenna unit A_n on X axis, $n \in 1, 2, ..., N$
for each antenna unit on Z axis **do**
  for $k \in -K, .. - 1, 0, 1, .., K$ **do**
    Calculate phase difference $\Delta\hat{\phi}$ and baseline B
    Calculate possible altitude value z_t based on InSAR
    Calculate possible y_t corresponding to z_t
    Gather the possible positions into set P
  end for
end for
Cluster point set P based on DBSCAN
Declare initial position cluster with highest density
Calculate (x_t, y_t, z_t) as the centroid of the highest density region

Compared to the naive hologram, the main contribution of our 3D localization scheme is the use of the InSAR approach to generate a series of possible locations, and select the most likely of these using DBSCAN. The approach proposed by Miesen et al. [16], computes a second naive hologram perpendicular to the first one to derive the 3D location estimation. We can call it *Cross Hologram*. Hologram generation in *Cross Hologram* is much more expensive than the computations we use (see Section III-C). Our approach also achieves higher localization accuracy, as we show in the next section.

IV. Experimental Results

We evaluate 3DinSAR in an indoor office environment with a size of $3m*3m*2m$ square to verify the performance of the localization scheme (see Figure 2*(a)*). An Impinj R420 COTS EPCglobal UHF C1G2 RFID reader [21] with one circular polarized 5.5 dBi gain Alien antenna [22] is used to communicate with six scattered target tags. The reader has the ability to successfully interrogate multiple tags during one inventory and divides their reflection signals based on the unique EPC code. We set the carrier frequency of the signal generated by the RFID reader to 920.625 MHz, and the transmission power to 30 dBm EIRP.

According to the Impinj reader hardware, it provides operations based on the EPC LLRP protocol [23] to support RF phase low level user data. We configure the reader to show the phase value with EPC code when the tag is

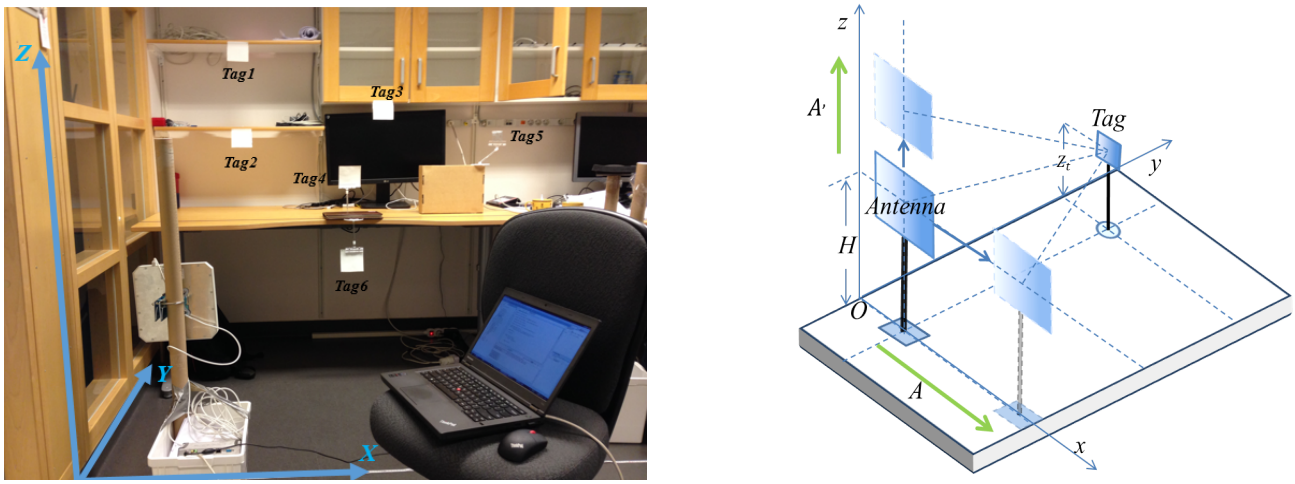

(a) (b)

Figure 2. (a) Indoor office measurement experiment setup. (b) Antenna movement directions. A and $A^{'}$ are the two virtual orthometic antenna arrays.

detected. The resolution of the output phase measurements is ≈ 0.0015 radians in theory but we observe it as actually 0.006 radians during our experiments. We implement the localization software using Python and run it on a Lenovo laptop with Intel Core i5 CPU at 2.6GHz and 16G memory.

The reader queries all six tags at the same time. The coordinate system is established as in Figure 2*(a)*. Figure 2*(b)* gives a more detail structure of our system. Following the basic idea of 3DinSAR as proposed above, we need two orthometric antenna arrays to provide sufficient phase measurements: one for holographic image creation and the other for phase difference based height determination. To this end, we move the antenna along the x-axis to generate synthetic aperture trajectory A and modify it on z-axis to acquire different heights (antenna array $A^{'}$) at $x = x_t$, where x_t is the tag's x-axis value.

A. Phase Measurement Errors

The quality of 3DinSAR depends on both the antenna position measurement accuracy and the phase measurement accuracy. Since we move the antenna to known positions, the phase measurement error caused by multipath effects will be the only factor that affects the accuracy. We collect more than 500 phase samplings on each antenna position at a height of $z = 0.63m$ from $x = 0.2m$ to $x = 1.9m$ with a $0.05\ m$ step to analysis the phase measurement errors and then calculate the 2D hologram locating results. The phase measurement error at each antenna position is following a low amplitude Gaussian distribution and we compute the final phase measurement by averaging over the values. The measurement results on each antenna position for Tag 6 are shown in Figure 3.

In this figure, the vertical distance between the curves for the measured and theoretical phases is a summation of system latency term c and multipath influence term c_{MP} as introduced in Equation1. We defined the "measurement" as an entire process which starts with the transmitting of inventory command and ends with the reception of tag reflection for one tag-reader communication pair. Hence c can be regarded as a constant and will not change during measurements for each tag-reader pair.

On the other hand, when the antenna moves to different positions during the experiments, the antenna pattern could have a negative effect if it is directional (for either the tag or the reader) and radiating in unsuitable direction. This could cause a multipath signal to be stronger than the signal of the shortest path. However, earlier works [10][14] have shown that the radiating orientation (which is defined as the angle between the reader antenna's polarization direction and the tag's antenna) does not have a big impact on the phase measurements. We consider such influence and other random reflection and environment interference all belong to the multipath influence term c_{MP}.

Ideally, the phase latency only depends on c and should be a constant for each tag/reader pair. However, the multipath influence term c_{MP} always exists and thus introducing randomly floating errors to the summation of phase latency. Such measurement errors will affect the positioning accuracy.

In this paper, we just retain the errors and directly use the averaged measurement values on each antenna position to evaluate the locating accuracy of 3DinSAR. Figure 4 shows the 2D holographic image generated by the original measured values for Tag 6. The resolution of the hologram method is $0.01\ m$ in a $3m \times 3m$ surveillance region.

As described in Section III-C, we need the phase difference for height estimation at $x = x_t$. However, since we move the antenna at discrete positions, there exists the possibility that the correct phase measurement value

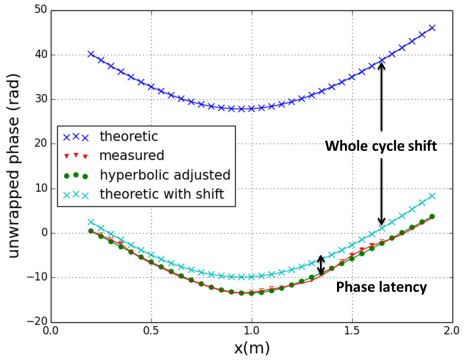

Figure 3. Measured phase data, theoretic phase data and hyperbolic fitting curve for Tag 6 when antenna is at z=0.63m.

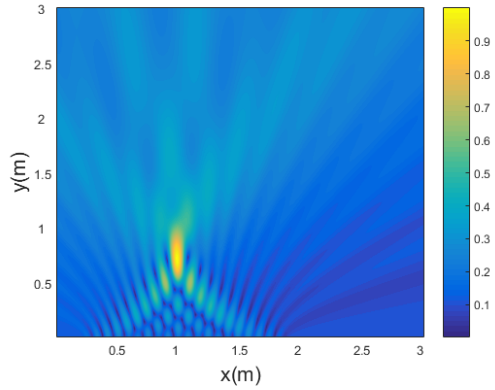

Figure 4. 2D Holographic image of Tag 6 at z=0.63m. The true position is (0.95,0.72,0.63). The estimated tag location is x=0.99m, l=0.72m.

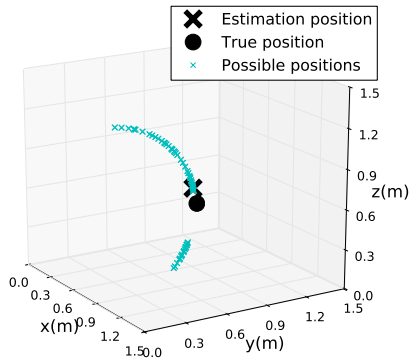

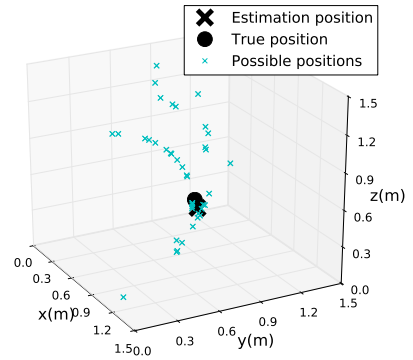

Figure 5. Basic 3DinSAR result for Tag 6 (top). 3DinSAR with more measurements for Tag 6 (bottom).

corresponding to $x = x_t$ cannot be provided. We perform a hyperbolic model fitting using function x: $\phi = f(x) = \sqrt{(\alpha x^2 + \beta x + \gamma)} + \epsilon$ on the incomplete phase measurement values to solve this problem. The ϵ here represents the unknown number of whole cycles phase offset between the theoretical phase curve and the measured one, as shown in Figure 3. We list the detail positioning results in the next section.

B. 3DInSAR Results

Based on the 2D hologram results, we firstly compare the results with *Cross Hologram* method to our 3DinSAR. To keep baseline $B > 0$, the z-axis antenna trajectory is created by moving the antenna along the z-axis from $0.63m$ to $0.97m$ with $0.01m$ steps for each tag. According to the experiment's communication range, we set the phase ambiguities k value from $-\lceil \frac{2B}{\lambda} \rceil$ to $\lceil \frac{2B}{\lambda} \rceil$, the density-based clustering initial scanning radius E and the minimum contains points $MinPts$ as $0.01m$ and 5. We use the mean of the Euclidean distances between the true positions Tag_p and the estimated positions $\hat{Tag}_p$ as the estimation error:

$$MD(\hat{Tag}_p) = \frac{\sum_{p=1}^{P} |Tag_p - \hat{Tag}_p|}{P} \tag{9}$$

We list the estimation errors for the two approaches in Table 1. The marker $*$ in Table I indicates that we do not count the results of Tag1 and Tag2 into the error evaluation for *Cross Hologram* method. It is because by observing the z-axis value, the most likely position already exceeds the surveillance region on the holographic image and hence the localization results are meaningless. Such phenomenon may happen when using a short aperture size (e.g. $0.63m$ to $0.97m$ for A' in Figure 2*(b)*) in comparison with the whole surveillance region ($0m$ to $3m$) to generate the naive hologram results. Since we implement the first antenna array (described in the previous section as A) with a long enough aperture ($0.2m$ to $1.9m$) in order to ensure the 2D positioning accuracy both for *Cross Hologram* and 3DinSAR, it obviously indicates that 3DinSAR scheme provides higher accuracy with identical phase measurement data when comparing to *Cross Hologram*. Additionally, 3DinSAR also

Table I
EXPERIMENTS RESULTS OF CROSS HOLOGRAM AND 3DINSAR

Actual Positions (m)	Cross Hologram	Basic 3DinSAR
(0.44, 1.2, 1.71)	(0.44, 1.74, 2.99)	(0.44, 1.624, 1.556)
(0.44, 1.2, 1.29)	(0.44, 0.92, 2.99)	(0.37, 1.304, 1.218)
(1.19, 1.18, 1.52)	(1.19, 1.21, 1.94)	(1.19, 1.306, 1.368)
(0.95, 0.95, 1.1)	(0.98, 0.88, 0.47)	(0.98, 1.157, 1.046)
(1.7, 0.95, 1.29)	(1.99, 1.14, 1.06)	(1.99, 1.319, 1.536)
(0.95, 0.72, 0.63)	(0.99, 0.3, 1.25)	(0.99, 0.666, 0.766)
Min Error (m)	0.416	0.144
Max Error (m)	0.749*	0.529
MD (m)	0.55*	0.281
Latency (s)	9.33	4.1

Table II
EXPERIMENTS RESULTS WITH MORE MEASUREMENTS 3DINSAR

Actual Positions (m)	More measurements 3DinSAR
(0.44, 1.2, 1.71)	(0.431, 1.263, 1.887)
(0.44, 1.2, 1.29)	(0.415, 1.063, 1.236)
(1.19, 1.18, 1.52)	(1.199, 1.308, 1.346)
(0.95, 0.95, 1.1)	(0.978, 1.006, 0.919)
(1.7, 0.95, 1.29)	(1.931, 0.779, 1.970)
(0.95, 0.72, 0.63)	(0.988, 0.719, 0.579)
Min Error (m)	0.063
Max Error (m)	0.736
MD (m)	0.243
Latency (s)	18.74

has lower latency, where the latency is denoted as the time consumption to execute the entire hologram generation and localization algorithm (excluding the phase acquisition period).

As a second experiment, we add measurements using several antenna trajectories parallel to the x-axis, at different heights to provide more measurements. The purpose is to evaluate if we can further improve the localization accuracy. We repeat the phase measurement by moving the antenna from $x = 0.2m$ to $x = 1.9m$ with a $0.05m$ step at the heights $0.85m$, $0.95m$, $1m$, $1.1m$ and $1.15m$. Each of the trajectories generates one holographic image, and for each such trajectory, all trajectories above that one is used to the information for the InSAR phase difference defined in Section III-C.

Table II shows the results. Utilizing more phase measurements from multiple antenna trajectories, the mean estimation error for the 6 tags is reduced to $0.243\ m$ with a minimum error of $0.063\ m$. Figure 5 shows the difference between the positioning results with basic 3DinSAR and with more measurements. The small blue crosses indicate all the possible positions. Black circles indicate the true positions, and black crosses are the estimated positions. From the figure we can derive that the probability to pick the true position increases with the measurement data. Figure 6 shows the final location results of the 6 tags by using more measurements and 3DinSAR.

Comparing with basic 3DinSAR, the computing time increases close to $20s$ for the calculation of the holographic images for all the trajectories when we use more measurements. In future work, we expect to further decrease the computation time by pre-estimating the angle of arrival and focus on the pixels in the estimated direction instead of traversing all the pixels. It would also be preferable to collect the phase measurements in an arbitrary and consecutive 3D curve instead of the straight line we used in this paper to analyze the performance of our method in more practical and complex environments.

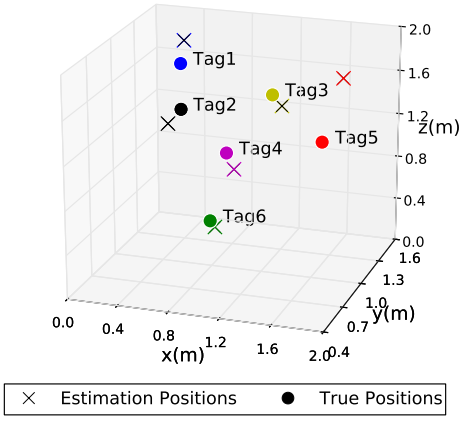

Figure 6. All the 6 Tags Localization Results

V. CONCLUSIONS

In this paper we propose an accurate object 3D localization scheme which is especially applicable for both portable readers and transport vehicles. Our system does not require reference tags and only one antenna is required to move in a known way in order to construct the synthetic arrays to implement the locating system. Our results using real hardware in an office show a localization result with a spatial median error of $0.24\ m$.

ACKNOWLEDGMENTS

This research is supported by Beijing Natural Science Foundation (No. 4122010), Beijing Science and Technology Innovation Program, International Program for Graduate Students of Beijing University of Technology and Beijing Engineering Research Center for IoT Software and System. We thank the reviewers and our shepherd Michael Goller for their valuable comments and helpful suggestions.

REFERENCES

[1] P. Hu, L. Li, C. Peng, G. Shen, and F. Zhao, "Pharos: Enable physical analytics through visible light based indoor localization," in *Proc.of ACM Workshop on Hot Topics in Networks*, 2013.

[2] D. Lymberopoulos, J. Liu, X. Yang, R. R. Choudhury, V. Handziski, and S. Sen, "A realistic evaluation and comparison of indoor location technologies: Experiences and lessons learned," in *ACM IPSN*, 2015, pp. 178–189.

[3] Y. Zhao and J. R. Smith, "A battery-free RFID-based indoor acoustic localization platform," in *IEEE RFID*, 2013, pp. 110–117.

[4] A. Furlan, S. Miller, D. Sorrenti, F. Li, and S. Savarese, "Free your camera: 3D indoor scene understanding from arbitrary camera motion," in *Proc.of BMVC*, 2013.

[5] B. Kim, P. Kohli, and S. Savarese, "3D scene understanding by Voxel-CRF," in *IEEE ICCV*, 2013, pp. 1425–1432.

[6] H. Malla, P. Purushothaman, S. V. Rajan, and V. Balasubramanian, "Object level mapping of an indoor environment using RFID," in *Proc.of UPINLBS*, 2014, pp. 203–212.

[7] J. Wang, F. Adib, R. Knepper, D. Katabi, and D. Rus, "RF-Compass: Robot object manipulation using RFIDs," in *ACM Mobicom*, 2013, pp. 3–14.

[8] L. Shangguan, Z. Yang, L. Alex, and Y. Liu, "Relative localization of RFID tags using spatial-temporal phase profiling," in *NSDI*, 2015.

[9] M. Scherhaufl, M. Pichler, and A. Stelzer, "Localization of passive UHF RFID tags based on inverse synthetic apertures," in *IEEE RFID*, 2014, pp. 82–88.

[10] L. Yang, Y. Chen, X.-Y. Li, C. Xiao, M. Li, and Y. Liu, "Tagoram: Real-time tracking of mobile RFID tags to high precision using COTS devices," in *ACM Mobicom*, 2014, pp. 237–248.

[11] J. Hightower, R. Want, and G. Borriello, "SpotON: An indoor 3D location sensing technology based on RF signal strength," *UW CSE 00-02-02, University of Washington, Department of Computer Science and Engineering, Seattle, WA*, 2000.

[12] F. Tlili, N. Hamdi, and A. Belghith, "Accurate 3D localization scheme based on active RFID tags for indoor environment," in *IEEE RFID-TA*, 2012, pp. 378–382.

[13] J. Maneesilp, C. Wang, H. Wu, and N. Tzeng, "RFID support for accurate 3D localization," *IEEE Transactions on Computers*, vol. 62, no. 7, pp. 1447–1459, 2013.

[14] T. Liu, L. Yang, Q. Lin, Y. Guo, and Y. Liu, "Anchor-free backscatter positioning for RFID tags with high accuracy," in *IEEE INFOCOM*, 2014, pp. 379–387.

[15] R. Miesen, F. Kirsch, and M. Vossiek, "Holographic localization of passive UHF RFID transponders," in *IEEE RFID*, 2011, pp. 32–37.

[16] R.Miesen, F.Kirsch, and M.Vossiek, "UHF RFID localization based on synthetic apertures," *IEEE Transactions on Automation Science and Engineering*, vol. 10, no. 3, pp. 807–815, 2013.

[17] J. Wang and D. Katabi, "Dude, where's my card? RFID positioning that works with multipath and non-line of sight," in *ACM SIGCOMM*, vol. 43, no. 4, 2013, pp. 51–62.

[18] Q. Lin, L. Yang, Y. Sun, T. Liu, X.-Y. Li, and Y. Liu, "Beyond one-dollar mouse: A battery-free device for 3D human-computer interaction via RFID tags," in *IEEE INFOCOM*, 2015, pp. 1661–1669.

[19] D. Massonnet and K. L. Feigl, "Radar interferometry and its application to changes in the earth's surface," *Review of Geophysics-Richmond Virginia Then Washington*, vol. 36, pp. 441–500, 1998.

[20] M. Ester, H.-P. Kriegel, J. Sander, and X. Xu, "A density-based algorithm for discovering clusters in large spatial databases with noise." in *Proc. of Knowledge Discovery and Data Mining*, vol. 96, no. 34, 1996, pp. 226–231.

[21] "Impinj,inc." http://www.impinj.com/.

[22] "Alien,inc." http://www.alientechnology.com.cn/upload/ALR-8696-C.

[23] EPCglobal, "Low level reader protocol (llrp)," 2010.